International Journal of
INTELLIGENT SYSTEMS AND APPLICATIONS IN ENGINEERING
ISSN:2147-6799 www.ijisae.org Original Research Paper

Framework for Classifying Long Bone Detection Using Image Processing Techniques

Selin Vironicka A[1], Dr. J. G.R. Sathiaseelan[2]

Submitted: 06/06/2022 **Accepted:** 10/09/2022

Abstract- Humans frequently have bone fractures, which can happen as a result of trauma to the bone, simple accidents, osteoarthritis, and bone cancer. Consequently, a critical component of the healthcare profession is the precise detection of bone fractures. In this research, bone fracture analysis is performed using X-ray pictures. The goal of this work is to create a fast and precise method for categorizing bone fractures based on the data obtained from x-ray pictures using image processing. The patients receive pictures of the broken bone, and processing systems such pre-processing, segmentation, edge detection, and feature extraction are used. The final classification of the analyzed pictures into fracture and nonfractured bone will evaluate the precision of various approaches. Our study demonstrates that the suggested strategy is straightforward and effective, making it desirable for ductile fracture identification and classification at a time when doctors and radiologists are interacting with an increasing number of patients and trying to reduce workload. In addition, this method outperforms state-of-the-art methods in positions of outcomes, run response period, and detecting accuracy.

1. Introduction

The human body's solid organs, or bones, serve as the guardians of several vital organs, including the brain, heart, lungs, and other vital organs. The 206 bones in the human body come in different sizes, forms, and configurations. The leg bones are the largest bones, and the hearing cranial bones are the tiniest bones. Humans frequently suffer from bone fractures. Accidents or any other situation during which the bones are subjected to heavy pressure can result in bone fractures. Oblique, complex, confluent, spiral, greenstick, and transverse bone fractures are among the several forms that can occur. X-rays, magnetic resonance imaging (MRI), computed tomography (CT),ultrasonography, and other forms of medical imaging technologies are able to determine various problems. Because it is the quickest and simplest approach for clinicians to examine damage to bones and muscles, X-rays and CT are most utilized generally in fracture detection. In order to evaluate how well a fracture is present and where it is located, doctors typically use x-ray scans. Machine learning and deep learning techniques are now used to diagnose medical issues that are occurring in real time [1, 2]. Additionally, a number of deep CNN models have been documented in the past to show how useful they are for a variety of applications [3,4].

In the present investigation, our goal is to accurately identify bone fractures so that the fracture may be properly treated and the extent of the bone fracture can be assessed. The noise that can be eliminated through image processing is particularly noticeable in X-ray pictures. The investigation of various forms of human bones is covered in a number of academic works. This is why Lu et alteam .'s [5] developed a deep CNN-based method for general fracture diagnosis. Utilizing preprocessing steps, a picture's performance is first enhanced. Following that, the dataset is expanded through data augmentation. A mean precision of 68.4% is employed by Ada-ResNeSt to classify broken and normal bone. Guan et al model.'s performance was improved on arm bone X-ray pictures in a different study [6]. They created a model for identifying fractures in arm bones. The primary alterations consist of three elements. First, a new backbone transnational corporations on the function pyramid structure is created in order to obtain additional fractural information.

[1] [1]*Research Scholar, Department of Computer Science, Bishop Heber College (Affiliated to Bharathidasan University), Tiruchirappalli, Tamilnadu, India*
mdselin93@gmail.com
[2]*Associate Professor, Department of Computer Science, Bishop Heber College (Affiliated to Bharathidasan University), Tiruchirappalli, Tamilnadu, India*
jgrsathiaseelan@gmail.com

Secondly, a picture preparation technique uses an opening approach and image pixel alteration to enhance the brightness of the source images.

An instantaneous abnormality detection system is produced as a result of image pre-processing, which includes actions like contrast development and noise deduction. The Gray Level Co-occurrence Matrix (GLCM) texture features are used in picture categorization difficulties. GLCM denotes the nonlinear fractional numerical data about the grey levels among adjacent pixels in a picture. Next we proposed a transfer learning, modified Faster R-CNN with rotating bounding box deep learning model for fracture detection and classification with Region Proposal Network (RPN). We evaluated the proposed model concerning detection and classification. We divide x-ray pictures of broken bones into 2 groups, fracture and non-fracture, and we also pinpoint the position of fractures using a rectangular box. Regarding classification and detection, the accuracy level attained by this method is 94.7%. Our research confirms that the suggested technique is straightforward and effective, making it valuable for fracture classification and dynamic detection at a time when doctors and radiologists are interacting with a growing number of patients and dealing with increased workload. In addition, when evaluated to state-of-the-art approaches, our strategy yields better results, run completion time, and recognition accuracy.

2. Problem Statement

The human body depends on bones to function. It facilitates people's movement from one location to the next. An incident or other event may result in a bone fracture. Treatment after a fracture is required as soon as feasible. To identify broken bones, an orthopaedic surgeon looks at an X-ray or CT scan image. Competence is necessary for the bone fracture diagnosing procedure. In order to aid an orthopaedic surgeon, a reliable and effective automated system that can analyze bone cracks in present must be developed. A number of research investigations have been done in the past to develop an automation process employing ML and DL. The absence of this ideal answer necessitated the use of hand-crafted features in the ML approach. The DL technique, in contrast, involves extracting characteristics and offers an improved diagnostic, but it has a higher processing cost and needs a sizable data to develop the model.

3. Related Work

A model based on the method of machine learning was created by Basha et al. [7] for the identification of bone fractures. The Gaussian filter is first used to enhance an X-ray image's quality. The clever edge technique is then used to find the edge. Finally, the broken sections are located using the Harris corner detection technique. This technique has a 92% accuracy rate for identifying fractured bone.

Built on several wavelet everyday transforms and median filtering, Tamara K [8] described four different stages of a discrete wavelet transform for the elimination of Gaussian noise from numerous medical images. When it comes to reducing noise from medical images, the suggested technique delivered satisfactory results. The PSNR, MSD, and NC outcomes are used to gauge how effective the suggested algorithm is.

A novel iris anti-counterfeit detection method is provided by Dian Li [9] and is based on an updated Gray Level Cooccurrence Matrix and a binary classification neural network (Modified-GLCM). The results of the experiment demonstrate that the recommended approach beats both the classic texture analysis methods using feature characteristics and the best result of LivDet-Iris2017. Additionally, they evaluate and assess the potential danger posed by the iris adverse example on the iris performing phrase detecting system utilising iris texture extraction.

For the purpose of detecting skull fractures, Lin et al. [10] created the fracture R-CNN (Region-based Convolutional Neural Network). To improve classification results, they used quicker R-CNN with prior medical skills.

An ensemble-based deep CNN model for detecting ankle fractures was created by Kitamura et al. [11]. For feature extraction, they use ResNet, InceptionV3, and Xception. With an accuracy of 81%, the ensemble-based model distinguishes between normal and cracks.

For the segmentation and detection of femoral neck fractures, Yang et al. [12] created two deep CNN systems. In training and testing, they divided the dataset into two sections, using 32,045 and 11,465 photos, correspondingly. First, a CNN with a cascade structure is used to extract the region of interest (ROI). The segmentation and identification process is then completed using a different CNN.

In another study, preprocessing was used to downsize a picture of a rib fracture to 128 128 333 pixels by Haitaamar et al. [13]. The ribs' cracked area was then located using a semantic classifier model. The CT scan image classification process was completed using the UNet model, which had an accuracy of 88.54%.

The Yolo 4 model was used by Nguyen et al. [14] to localise broken bones. Additionally, the data augmentation approach was used, and the model's performance was assessed against the baseline and supplemented datasets. This technique can distinguish between fractured and healthier areas on an unique dataset with an accuracy of 81.94%.

Asma Alzaid [15] 2022 In this study, we use simple radiographs to evaluate how well current classification schemes work on binary and multi-class problems (fracture kinds). The effectiveness of object detection algorithms using one- and two-stage DL designs was also assessed. A thorough analysis of several techniques revealed that Resnet50 can identify fracture types with a 90% accuracy and detect PFFs with an accuracy of 91%. The fracture location could roughly be seen using the CAM technique. With a localization accuracy of 78%, Faster RCNN forecasted a smaller frame for the fracture area.

4. Proposed Method

The hospital provides the X-ray/CT scans, which show both pictures of healthy and pictures of broken bones. Using pre - processing steps like RGB to grayscale converting and enhancing them with filtering algorithms in the first stage will reduce the image's noise. Following removing noise, it uses the Gray Level Co-occurrence Matrix (GLCM) texture features extraction approach to turn each image into a set of features. The classification method is then developed using the features that were extracted. Lastly, the suggested system's effectiveness and accuracy are assessed. Figure 1 below demonstrates the proposed scheme's flow chart for identifying bone fractures in X-ray pictures.

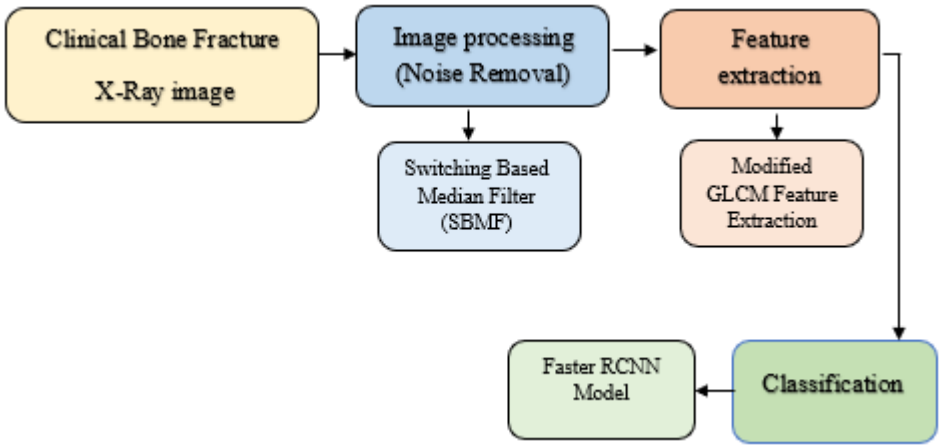

Figure1- The process flow diagram for identifying bone fractures in CT and X-ray pictures

5) Image Pre-Processing

Image processing techniques for removal of noise, feature extraction, and classification are essential for the effectiveness of such processes in computer-aided computer vision assessment. The patients receive the X-ray/CT scans, which show both pictures of healthy and pictures of broken bones. Using pre-processing methods like RGB to grayscale conversion and the improved median filter to eliminate noise from the photograph in the first step.

The elimination of noise from images is a crucial problem. Unwanted interference in a photograph is known as noise. Digital photos can shape several noise sources, such as capture noise, resulting in light changes, such as excessive or inadequate light, and noise correction due to numerically accurate constraints and theoretical methodologies. (e.g., π = 3. 142..). The resolution of a digital photo, which depicts the actual scene, is sometimes limited by sampling and noise pollution.

There are numerous terms used to describe noise in photographs. For image processing, the mainly two noise types, salt and pepper noise and Gaussian noise, are frequently utilised. Salt and pepper noise, often referred to as impulsive noise, is caused by the erroneous addition of either pure white or pure black pixels to the image. This noise is typically caused by the photographic sensor failing. Gaussian noise, commonly referred to as additive noise, is noise of random level with a Gaussian or regular distribution function. Random activities in electrical equipment are typically to blame.

a) Switching Based Median Filter (SBMF) Algorithm

We presume that the picture is X×Y in size and has a $PR \in [0,255]$ 8-bit grayscale pixel resolution. The centre pixel in a 3x3 window, $Win_{x,y}^{(i)}$at (x,y), is defined as $i(x,y)$ and its neighbours as $\{i_k(x,y)\}_{l=1}^{8}$. The filtered outcome for $i(x,y)$ in the traditional switching median filter $j(x,y)$ is provided by,

$$j(x,y)\begin{cases} = median(Win_{x,y}^{(i)}); |median(Win_{x,y}^{(i)}) - i(x,y)| > threshold \\ = i(x,y) \qquad ; otherwise \end{cases}$$

A binary flag picture serves as the impulse detector's output $\{fi(x,y)\}$, anywhere the $fi(x,y) =$ 1indicates that the pixel $i(x,y)$ is noisy; for noiseless pixel $fi(x,y) = 0$.

The noisy pixels are initially recognised in the suggested technique from the pixel values in the frame $Win_{x,y}^{(i)}$,, and if the image is determined to be noisy repeatedly, it is

changed with the median of the noise-free pixels in the image after being evaluated in the larger frame.

The proposed filter performs better than the other two median and Gaussian filters, according to study results. Quality photo assessment is a crucial step in the processing of photographic files. In this research, the metrics (MSE, PSNR, and SSIM) are used to obtain the best value metric. Utilizing the aforementioned metrics, the quality of the obtained image has also been assessed.

6) Feature Extraction

a) Modified-Glcm

It is possible to extract the texture features at a large scale from the picture and to gather more integrated something among individual spots. This will be extremely beneficial for real-time biometric authentication. This research suggests a revised technique on GLCM as a remedy for the current inadequacies of GLCM and the textural features of coloured contact lenses. It is known as Modified-GLCM. The GLCM texture feature range can be increased using this technique.

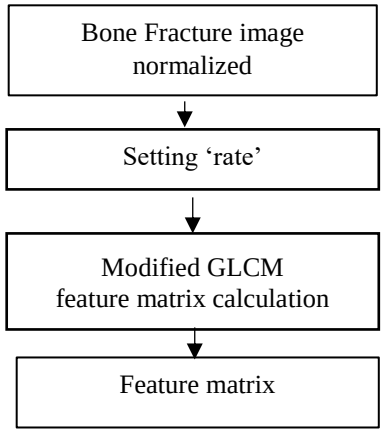

Figure 2- Calculation process of Modified-GLCM algorithm.

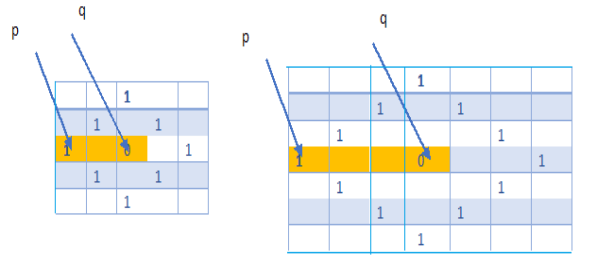

$rate = |p_i - q_i| + |p_j - q_j| = 2$ (a) rate=2 $rate = |p_i - q_i| + |p_j - q_j| = 3$ (a) (b) rate =3

Figure 3- Distance Measurement

Fig. 2 depicts the Modified-GLCM method, together with the rate setting and Modified-GLCM feature matrix calculations. We create a parameter named rate to signify the size of the Modified-features, GLCM's as seen in Fig. 3. In the grey image, rate stands in for the Manhattan distance among two aspects with the grey values p and q. L1 norm is used to represent the length as in

$$rate = |p_i - q_i| + |p_j - q_j| \quad (1).$$

anywhere i and j represent the digit of rows and columns of the two elements whose gray level is p and q.In this case, Modified-GLCM is evaluated for all elements pairings that satisfy the scale of the features requirements rather than in a specific direction. The calculation of Modified-GLCM is expressed as follows.

$$Modified\ GLCM(p,q) =$$

$$\sum_{\substack{p\epsilon G \\ q\epsilon G}} \begin{cases} 1, if\left(|p_i - q_i| + |p_j - q_j| = rate\right) \cap \\ \left((|p_i - q_i| - |p_j - q_j|) \leq 0\right) \\ 0, others \end{cases}$$

where G means the gray level map with size of m×n, p and q are the elements in the gray level map, $p \in G\ (G\ (i,j) = p, i \in (1,m), j \in (1,n))$ means the gray level of the element in G is p, $|p_i - q_i| + |p_j - q_j|$= rate means that the elements with gray levels p and q meet the given rate.

if $|p_i - q_i| - |p_j - q_j|) \leq 0$ it means that the element with gray level p is at the upper left of the element with gray level q.

Statistics are used to determine the frequency of element pairs that satisfy the scale requirements for the features. For example, Modified-GLCM (1, 1) indicates the number of (1, 1) component pairs in the gray scale image when rate = 2. It can be concluded that Modified-GLCM has a longer neighbourhood and more calculations orientations than GLCM by evaluating the two models that were derived from the identical grey level image in Figs. 2 and 3. Modified-GLCM filters away certain duplicate statistical values, such as band textures in a limited region that have the same grey level, and recovers more location data about picture patterns than GLCM does. The (1, 1) element pairings in the downward motion are discovered to be excluded from the analysis. Please take note that we are more interested in the texture's edge, structure, and overall case. The external group texture computation can be simplified in this fashion.

A further benefit of Modified-GLCM over GLCM is that it has more thorough statistical image data, which can be inferred from the method of calculation of the aforementioned technique. While GLCM can only compute one direction once when rate is 3, Modified-GLCM may extract texture information in 12 directions evenly distributed by 360 degrees. This is excellent news for the full separation of image characteristics.

Modified GLCM in SVM approach reached a classification accuracy of 95.22% with sensitivity of 95.06%, specificity of 95.38%, precision of 95.49% and F1 score of 95.27, Random Forest approach reached a classification accuracy of 94.15% with sensitivity of 93.75%, specificity of 94.63%, precision of 95.48% and F1 score of 94.61; Logistic Regression approach reached a classification accuracy of 85.94% with sensitivity of 92.40%, specificity of 81.33%, precision of 77.93% and F1 score of 84.55; Decision tree approach reached a classification accuracy of 85.73% with sensitivity of 82.70%, specificity of 88.84%, precision of 88.39% and F1 score of 85.45%. Furthermore, the improved GLCM with SVM performs significantly better than the other three approaches, which is optimistic given the greatest challenge of the MURA data facture identification.

7) Classification and Detection

The Faster-RCNN model was used to develop an automatic long bone fracture recognition and organization system. The VGG-16 structure was chosen as the basic network in the suggested process to improve a feature map that will provide suggestions for crack area classification and detection.

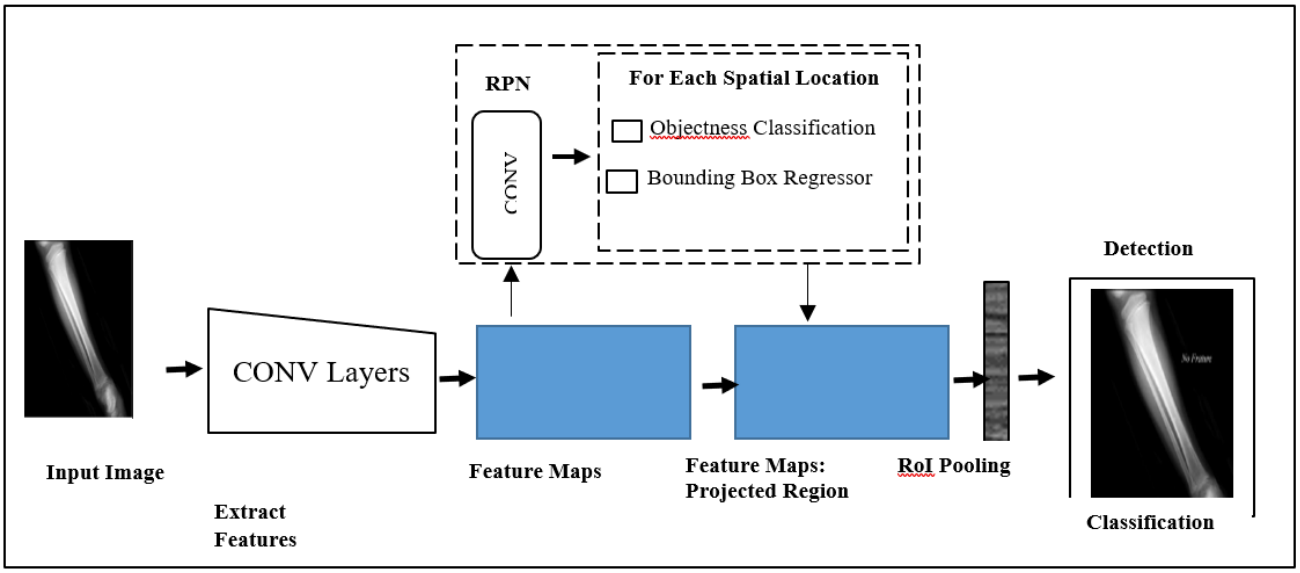

Figure 4: A Visual representation of proposed scheme.

A.CNN Network

Figure 4 illustrates the use of a transfer learning Faster R-CNN deep convolutional neural network at this level. The three neural networks that make up the Faster RCNN model are described here.

- Feature Network
- Detection Network
- Region Proposal Network

a) Feature Network

Normally, the term "Feature Network" refers to a system that eliminates several levels from classifier pictures during the last/top classification. This network's objective is to extract useful features from the photos. The outcome of this system retains the form and hierarchy of the main image.

b) Detection Network

The RPN and Feature Network provide input to the Detection Network, also known as the RCNN network, which then generates the very last class and bounding box. There are four densely integrated or dense levels in this structure. First layer is employed for classification, second layer is utilised for regression, and the final two levels are shared, stacking standard layers. To allow the boundaries squares to differentiate solely inside the RPN and the Recognition System require training, the characteristics are reduced in accordance with the bounding points.

c) Region Proposal Network

The RPN typically consists of a three-layer simple network. One component in particular feeds information into two other layers: the first layer for categorization and the third and second layers for regress bounding boxes. Bounding boxes, or regions of interest, are made using the RPN network. There is a good likelihood that there is an object in this area of interest. Multiple bounding boxes identified by the resolution value location of 2 vertical approaches, which have two sorts of data, are used to evaluate the performance of RPN. The possibilities for the likelihood that a fracture is depicted inside the box may be omitted, are 0, 1, and -1.

d) Training

In this phase, inception v2 (Version 2) networks are used to retrain the Faster RCNN's top layer. Training will keep

going until the loss rate reaches 0.0005%. We trained the suggested technique to minimise convolution layer values, proposition region weights, and convolution layer filters using gradient descent stochastic (SGD). The variables are updated by stochastic gradient descent (SGD) for each instance of learning XCi) and label yCi).

$$\beta = \beta - \eta.\nabla\beta k(\beta; x^i; y^i) \qquad (1)$$

Where β erudite rate and new knowledge rate are assumed. A procedure known as anchor boxes initially generates a number of bounding boxes before using them to train the RPN. An anchor is a single "pixel" created from a feature picture. The group of pixels in the primary picture's rectangular box known as an anchor box. On the segmentation process, the anchors box is evenly distributed along the X- and Y-axis measurements. A scalar form rather than the entire feature vector alone is the source needed to produce an anchor box first from information generating layer. Depending on every anchor, multiple rectangle boxes of various dimensions and shapes are generated. Normally, 9 boxes with a 3*3 size contents each box are made.

Technique known as Non-Maximum Suppression (NMS) was used during the initial stage of decrease. Boxes that overlay adjacent boxes with higher values are removed by NMS. The classification and detection threshold was set at 0.5. In the learning phase, close to 2,000 boxes are acquired. These boxes, together with their results, are sent directly to the Detection Network during the system testing. When moving to the classifier by filtering to about 256, the two thousand boxes are once again reduced throughout the training phase. IOUs are obtained from all anticipated boxes as well as regression coefficients boxes when we build RPN labels (such as forefront, backgrounds, and ignores). The IOUs are utilized to produce the labelling, which can be either fracture or normal. In addition, 256 boxes are produced, each of which includes an area of interest in both the background and foreground.

$$IoU = \frac{area\_overlap}{area\_union} \qquad (2)$$

Cross-entropy is calculated by disregarding the boxes with -1 values. The bounding box is generated using an RPN network, which is then scaled to fit all around lengthy bone defects. The regressive anchoring box refers to this. In order to do this, a fracture must be identified and diagnosed. Losses must be recovered using backpropagation, and calculations for training must be made it after every stage. The expected anchoring box and regression coefficients box's central pixel are used to calculate a routing path, which is then normalised by size for the anchoring box.

The LI smooth expression is used to compute the depreciation. It is impossible for O to distinguish the usual loss of LI. By employing a loss of L2 past O, smooth loss of Ll gets around this. named sigma and assigned an L2 loss intensity of blew.

$$abs(N) < \frac{1}{S^2} \qquad (3)$$

$$L = \frac{(d \times S)^2}{2} \text{ Else} \qquad (4)$$

$$L = abs(d) - \frac{1}{(2*S)^2} \qquad (5)$$

8) Proposed Work

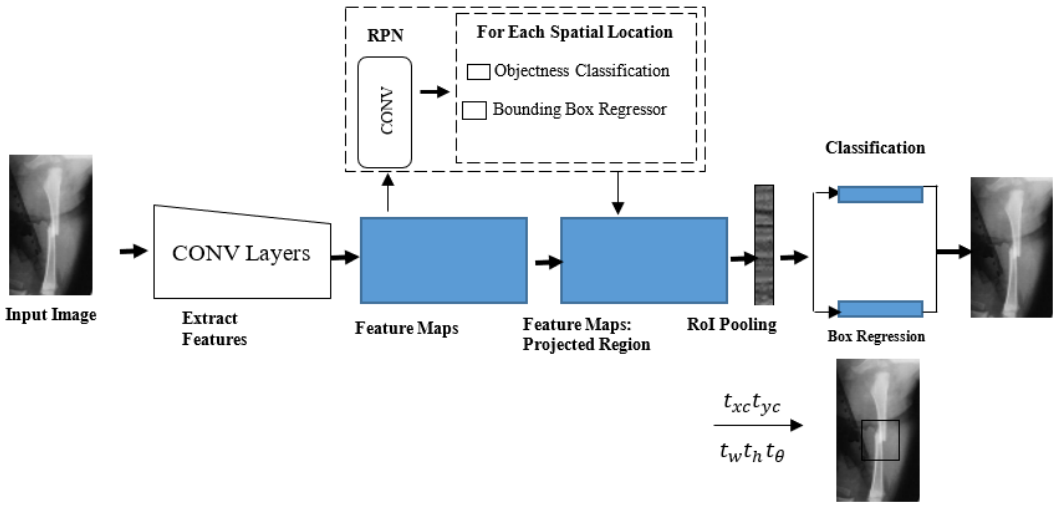

Figure 7- Block diagram of Proposed method.

Practically identical tasks are performed by RPN and R-CNN, although in varied contexts. As an illustration, they make improvements to the bounding box coordinates where a fracture is expected to stop in order to better match the shape of the fracture. The two differ in that RPN utilizes the whole features map created from the image data, whereas RCNN only uses a select few part areas in the feature maps matching to suggestion boxes for final

bounding box estimates. The following sections will go over the adjustments within of each component required for rotating bounding box estimations.

Before delving into the specifics of the Faster R-CNN, it is useful to list the methods of rotational bounding box and anchor box. As was already mentioned, orientated rectangular boxes will be used to detect fractures. In order to compensate for box orientation, a further parameter of angle (0) is introduced for this bounding box description in addition to the four features typical of centre point coordinates (xc, ye), width (w), and height (h). This angle, which ranges from -90° to 90°, is specified as the angle between the bigger side of the bounding box and the positively vertical axis. It is also important to note that the bounding box's width is indeed smaller than its height. Anchor boxes are a collection of already-defined, rotating bounding boxes that have a specific scale, aspect ratio, and angle. They are evenly dispersed around the picture and will serve as examples when the RPN stage generates proposal boxes.

The following equations (6) through (10) will be used to determine the offset value between the allocated anchor boxes and the ground truth box. The scale-invariant shift between centre coordinates and the log-space height-width shift is shown in the (6) to (9) equations. The rotating angle is also shown in radian directions in the tenth equation. The branching or regressive will develop the ability to forecast those coordinates. Later, an anchor box will be transformed using the projected offset amounts.

$$t_x = ((x - x_a)/w_a \quad (6)$$

$$t_y = ((y - y_a)/h_a \quad (7)$$

$$t_w = bg(w/w_a) \quad (8)$$

$$t_h = bg(h/h_a) \quad (9)$$

$$t_\theta = (\theta - \theta_a) \times \frac{\pi}{180^\circ} \quad (10)$$

Where $x_a, y_a\ w_a, h_a,$ and θ_a are x,y centre co-ordinates, width and height orientation of anchor box respectively. RPN only provides coarse bounding boxes that might contain fracture, while having a bounding box regression branch. The main cause is because RPN must employ high-variance anchor boxes in order to forecast prospective boxes.

9.Results

The suggested technique's findings are illustrated using the identification and categorization of cracks in x-ray pictures.

Table 1: Concept Prediction for Detection and Classification in X-Ray Pictures of Fracture and Non-Fracture

Bone1 image

Result (Fracture 99%)
Type : wedge fracture

Bone2 image

Result (Fracture 98%)
Type : Transverse fracture

Bone3 Image

Result(Fracture: 93%)
Type : oblique fracture

Bone4 image

Result (No Frature)
Type : No Frature

a) Classification Results

Table 2. Classification-related Prediction

Sno	Prediction	Calculation	Exiting work	Proposed work
1	Sensitivity	30/(30+1)	96.7%	98.6%
2	Specificity	19+(19+2)	90.4%	92.7%
3	Precision	30(30+1)	96.7%	98.6%
4	Accuracy	(30+19)/(30+1+19+2)	94%	96.1%
5	FI Score	2(96.7)(96.7)/(96.7+96.7)	96.7%	98.6%

Figure 5- Graphical representation of Classification Results

Table 3. Comparison with other Papers

Reference number	Year	Technique	Dataset	Accuracy
[15]	2020	Convolutional neural network (CNN)	Musculoskeletal X-Ray Images	81%
[16]	2020	encoder-decoder structured neural network	femur fracture in pelvic X-ray images	86.78%
[17]	2020	convolutional neural network (CNN)	proximal femur fracture X-Ray Image	84%
[18]	2021	deep learning-based pertained models	Shoulder X-Ray Images	84%
[19]	2022	models for object recognition based on deep learning	wrist X-ray images	86%
[20]	2022	Support Vector Machine (SVM) and K-Nearest Neighbour (KNN)	Fracture Bones in X-ray Images	90%
[21]	2022	Deep Neural Networks (DNN)	X-ray pictures of broken bones	93%
Exiting work	2022	Faster R-CNN deep learning	X-ray images of long broken bones	94%
Proposed work	2022	Modified Faster R-CNN deep learning with rotated bounding box	X-ray images of long broken bones	96.1%

Applying Modified Faster-RCNN to the long bones fractures data allows for classification and detection evaluation, as demonstrated in Table 1. The source image is displayed in the first column in the table, while the output in terms of classification and detection is displayed in the second chart. The predicted outcomes of the model's predictions with regard to classification are displayed in Table 2. The system has attained a high level of classification accuracy. Pre-processing duration was shortened in the current study by employing the suggested technique. Figure 6 displays an accuracy compared with other region studies. The main goal of this project is to use deep learning to identify and categorise long bone fractures. This method is offered to treat bone illnesses, which are also known as broken bones. It divides fractures into two categories: fractures and non-fractures. All previous techniques' performances have been contrasted and examined.

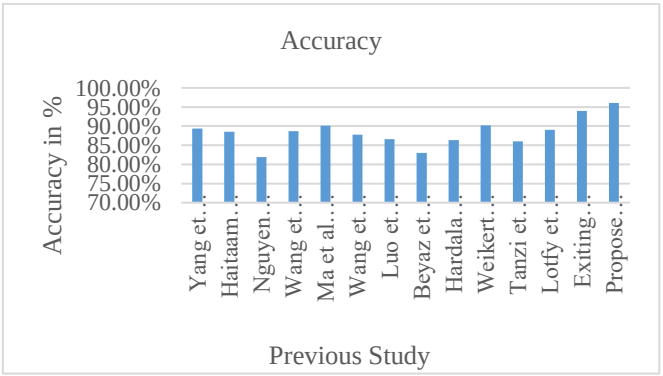

Figure 6- Accuracy Comparison Graph

10.Conclusion

This paper presents a system-oriented evaluation method for the detection of bone fracture utilising X-ray/CT pictures. Pre-processing to reduce noise is where it begins. A series of photos were used to test the approach, and the outcomes were assessed using GLCM elements. In order to automatically recognise and classify bone fractures in x-ray pictures, this classification effort recommends using a transfer learning performance. The modified Faster-RCNN with rotating bounding box deep learning model is used to locate the fracture zone and divide it into 2 modules fracture and non-fracture with size. The foundation network for the modified Faster-RCNN model with rotating bounding box approach was a deep convolutional network design known as VGG-16. The recommended approach successfully recognises lengthy broken bone by using a bounding box. It is possible to

extend this study to examine different types of long bone fractures. This work can be further enhanced to increase the method's effectiveness and output.

References

[1] Amirkolaee, Hamed Amini, Dmitry Olegovich Bokov, and Himanshu Sharma. "Development of a GAN architecture based on integrating global and local information for paired and unpaired medical image translation." Expert Systems with Applications 203 (2022): 117421.

[2] Singh, Law Kumar, Hitendra Garg, and Munish Khanna. "Deep learning system applicability for rapid glaucoma prediction from fundus images across various data sets." Evolving Systems (2022): 1-30.

[3] Garg, Hitendra, Neeraj Gupta, Rohit Agrawal, Shivendra Shivani, and Bhisham Sharma. "A real time cloud-based framework for glaucoma screening using EfficientNet." Multimedia Tools and Applications (2022): 1-22.

[4] Yu, Yang, Maria Rashidi, Bijan Samali, Masoud Mohammadi, Thuc N. Nguyen, and Xinxiu Zhou. "Crack detection of concrete structures using deep convolutional neural networks optimized by enhanced chicken swarm algorithm." Structural Health Monitoring (2022): 14759217211053546.

[5] Lu, Shuzhen, Shengsheng Wang, and Guangyao Wang. "Automated universal fractures detection in X-ray images based on deep learning approach." Multimedia Tools and Applications (2022): 1-17.

[6] Guan, Bin, Guoshan Zhang, Jinkun Yao, Xinbo Wang, and Mengxuan Wang. "Arm fracture detection in X-rays based on improved deep convolutional neural network." Computers & Electrical Engineering 81 (2020): 106530.

[7] Basha, Cmak Zeelan, M. Ravi Kishore Reddy, K. Hemanth Sai Nikhil, P. S. M. Venkatesh, and A. V. Asish. "Enhanced computer aided bone fracture detection employing X-ray images by Harris Corner technique." In 2020 Fourth International Conference on Computing Methodologies and Communication (ICCMC), pp. 991-995. IEEE, 2020.

[8] Al-Shayea, Tamara K., Constandinos X. Mavromoustakis, Jordi Mongay Batalla, George Mastorakis, Mithun Mukherjee, and Evangelos Pallis. "A Novel Gaussian in Denoising Medical Images with Different Wavelets for Internet of Things Devices." In GLOBECOM 2020-2020 IEEE Global Communications Conference, pp. 1-6. IEEE, 2020.

[9] Dian Li, Cheng Wu and Yiming Wang, “A Novel Iris Texture Extraction Scheme for Iris Presentation Attack Detection”, Journal of Image and Graphics, Vol. 9, No. 3, pp.1-12, 2021.

[10] Modiya, P., & Vahora, S. (2022). Brain Tumor Detection Using Transfer Learning with Dimensionality Reduction Method. International Journal of Intelligent Systems and Applications in Engineering, 10(2), 201–206. Retrieved from https://ijisae.org/index.php/IJISAE/article/view/1310

[11] Lin, Xian, Zengqiang Yan, Zhuo Kuang, Hang Zhang, Xianbo Deng, and Li Yu. "Fracture R-CNN: An anchor-efficient anti-interference framework for skull fracture detection in CT images." Medical Physics (2022).

[12] Kitamura, Gene, Chul Y. Chung, and Barry E. Moore. "Ankle fracture detection utilizing a convolutional neural network ensemble implemented with a small sample, de novo training, and multiview incorporation." Journal of digital imaging 32, no. 4 (2019): 672-677.

[13] Yang, Lv, Shan Gao, Pengfei Li, Jiancheng Shi, and Fang Zhou. "Recognition and Segmentation of Individual Bone Fragments with a Deep Learning Approach in CT Scans of Complex Intertrochanteric Fractures: A Retrospective Study." Journal of Digital Imaging (2022): 1-9.

[14] Haitaamar, Zineddine N., and Nidhal Abdulaziz. "Detection and Semantic Segmentation of Rib Fractures using a Convolutional Neural Network Approach." In 2021 IEEE Region 10 Symposium (TENSYMP), pp. 1-4. IEEE, 2021.

[15] Nguyen, Hoai Phuong, Thi Phuong Hoang, and Huy Hoang Nguyen. "A deep learning based fracture detection in arm bone X-ray images." In 2021 International Conference on Multimedia Analysis and Pattern Recognition (MAPR), pp. 1-6. IEEE, 2021.

[16] Alzaid, Asma, Alice Wignall, Sanja Dogramadzi, Hemant Pandit, and Sheng Quan Xie. "Automatic detection and classification of peri-prosthetic femur fracture." International Journal of Computer Assisted Radiology and Surgery 17, no. 4 (2022): 649-660.

[17] Hardalaç, Fırat, Fatih Uysal, Ozan Peker, Murat Çiçeklidağ, Tolga Tolunay, Nil Tokgöz, Uğurhan Kutbay, Boran Demirciler, and Fatih Mert. "Fracture Detection in Wrist X-ray Images Using Deep Learning-Based Object Detection Models." Sensors 22, no. 3 (2022): 1285.

[18] Varoquaux, Gaël, and Veronika Cheplygina. "Machine learning for medical imaging: methodological failures and recommendations for the future." NPJ digital medicine 5, no. 1 (2022): 1-8.

[19] Yang, Lv, Shan Gao, Pengfei Li, Jiancheng Shi, and Fang Zhou. "Recognition and Segmentation of Individual Bone Fragments with a Deep Learning Approach in CT Scans of Complex Intertrochanteric Fractures: A Retrospective Study." Journal of Digital Imaging (2022): 1-9.

[20] Nguyen, Hoai Phuong, Thi Phuong Hoang, and Huy Hoang Nguyen. "A deep learning based fracture detection in arm bone X-ray images." In 2021 International Conference on Multimedia Analysis and Pattern Recognition (MAPR), pp. 1-6. IEEE, 2021.

[21] Haitaamar, Zineddine N., and Nidhal Abdulaziz. "Detection and Semantic Segmentation of Rib Fractures using a Convolutional Neural Network Approach." In 2021 IEEE Region 10 Symposium (TENSYMP), pp. 1-4. IEEE, 2021

[22] M. J. Traum, J. Fiorentine. (2021). Rapid Evaluation On-Line Assessment of Student Learning Gains for Just-In-Time Course Modification. Journal of Online Engineering Education, 12(1), 06–13. Retrieved from http://onlineengineeringeducation.com/index.php/joee/article/view/45

[23] Wang, Mengxuan, Guoshan Zhang, Bin Guan, Mingyang Xia, and Xinbo Wang. "Multiple Reception Field Network with Attention Module on Bone Fracture Detection Task." In 2021 40th Chinese Control Conference (CCC), pp. 7998-8003. IEEE, 2021.

[24] Ma, Yangling, and Yixin Luo. "Bone fracture detection through the two-stage system of Crack-Sensitive Convolutional Neural Network." Informatics in Medicine Unlocked 22 (2021): 100452.

[25] Wang, Mengxuan, Jinkun Yao, Guoshan Zhang, Bin Guan, Xinbo Wang, and Yueming Zhang. "ParallelNet: Multiple backbone network for detection tasks on thigh bone fracture." Multimedia Systems 27, no. 6 (2021): 1091-1100.

[26] Luo, Jun, Gene Kitamura, Emine Doganay, Dooman Arefan, and Shandong Wu. "Medical knowledge-guided deep curriculum learning for elbow fracture diagnosis from x-ray images." In Medical Imaging 2021: Computer-Aided Diagnosis, vol. 11597, pp. 247-252. SPIE, 2021.

[27] Meneses, B., E. L. Huamani, M. Yauri-Machaca, J. Meneses-Claudio, and R. Perez-Siguas. "Authentication and Anti-Duplication Security System for Visa and MasterCard Cards". International Journal on Recent and Innovation Trends in Computing and Communication, vol. 10, no. 7, July 2022, pp. 01-05, doi:10.17762/ijritcc.v10i7.5558.

[28] Beyaz, Salih, Koray Açıcı, and Emre Sümer. "Femoral neck fracture detection in X-ray images using deep learning and genetic algorithm approaches." Joint diseases and related surgery 31, no. 2 (2020): 175.

[29] Hardalaç, Fırat, Fatih Uysal, Ozan Peker, Murat Çiçeklidağ, Tolga Tolunay, Nil Tokgöz, Uğurhan Kutbay, Boran Demirciler, and Fatih Mert. "Fracture Detection in Wrist X-ray Images Using Deep Learning-Based Object Detection Models." Sensors 22, no. 3 (2022): 1285.

[30] Weikert, Thomas, Luca Andre Noordtzij, Jens Bremerich, Bram Stieltjes, Victor Parmar, Joshy Cyriac, Gregor Sommer, and Alexander Walter Sauter. "Assessment of a deep learning algorithm for the detection of rib fractures on whole-body trauma computed tomography." Korean Journal of Radiology 21, no. 7 (2020): 891.

[31] Garg, D. K. . (2022). Understanding the Purpose of Object Detection, Models to Detect Objects, Application Use and Benefits. International Journal on Future Revolution in Computer Science &Amp; Communication Engineering, 8(2), 01–04. https://doi.org/10.17762/ijfrcsce.v8i2.2066

[32] Tanzi, Leonardo, Enrico Vezzetti, Rodrigo Moreno, Alessandro Aprato, Andrea Audisio, and Alessandro Massè. "Hierarchical fracture classification of proximal femur X-Ray images using a multistage Deep Learning approach." European journal of radiology 133 (2020): 109373.

[33] Lotfy, Mayar, Raed M. Shubair, Nassir Navab, and Shadi Albarqouni. "Investigation of focal loss in deep learning models for femur fractures classification." In 2019 International Conference on Electrical and Computing Technologies and Applications (ICECTA), pp. 1-4. IEEE, 2019.